

1       **Variations of Cloud Condensation Nuclei (CCN) and Aerosol**  
2       **Activity during Fog-Haze Episode: a Case Study from Shanghai**

3  
4       Chunpeng Leng <sup>a</sup>, Deqin Zhang <sup>a</sup>, Qun Zhang <sup>a</sup>, Chen Xu <sup>a</sup>, Tiantao  
5       Cheng <sup>a,b</sup>, Renjian Zhang <sup>c</sup>, Jun Tao <sup>d</sup>, Jianmin Chen <sup>a,b</sup>, Shuping Zha <sup>a</sup>,  
6       Yunwei Zhang <sup>a</sup>, Xiang Li <sup>a</sup>, Lingdong Kong <sup>a</sup>, Wei Gao <sup>e</sup>

7  
8       a. Shanghai Key Laboratory of Atmospheric Particle Pollution and  
9       Prevention (LAP<sup>3</sup>), Department of environmental science and  
10       engineering, Fudan University, Shanghai 200433, China;

11       b. Fudan-Tyndall Centre, Fudan University, Shanghai 200433, China;

12       c. Key Laboratory of Region Climate-Environment Research for  
13       Temperate East Asia, Institute of Atmospheric Physics, Chinese  
14       Academy of Sciences, Beijing 100029, China;

15       d. South China Institute of Environmental Sciences, Ministry of  
16       Environmental Protection, Guangzhou 510655, China;

17       e. Shanghai Meteorological Bureau, Shanghai 200030, China;

18  
19  
20       \* Corresponding authors: Tiantao Cheng, Jianmin Chen;

21       Tel: (86) 21-65643230; fax: (86) 21-65642080;

22       Email: [ttcheng@fudan.edu.cn](mailto:ttcheng@fudan.edu.cn), [jmchen@fudan.edu.cn](mailto:jmchen@fudan.edu.cn)

23 **Abstract**

24 Measurements of Cloud condensation nuclei (CCN), condensation nuclei  
25 (CN) and aerosol chemical composition were performed simultaneously  
26 at an urban site of Shanghai from 6 to 9 November 2010. The variations  
27 of CCN number concentration ( $N_{CCN}$ ) and aerosol activity (activated  
28 aerosol fraction,  $N_{CCN}/N_{CN}$ ) were examined during a fog-haze  
29 co-occurring event. Anthropogenic pollutants emitted from vehicles and  
30 unfavorable meteorological conditions such as low planetary boundary  
31 layer (PBL) height exerted a great influence on  $PM_{2.5}$  and black carbon  
32 (BC) loadings.  $N_{CCN}$  at 0.2% supersaturation (SS) mostly fell in the range  
33 of 994 to 6268  $cm^{-3}$ , and the corresponding  $N_{CCN}/N_{CN}$  varied between  
34 0.09 and 0.57.  $N_{CCN}$  and  $N_{CCN}/N_{CN}$  usually were higher in hazy case due  
35 to increased aerosol concentration in the accumulation mode (100-500  
36 nm), and lower in foggy-hazy and clear cases. BC mass concentration  
37 posed a strong positive effect on  $N_{CCN}$  in foggy-hazy and hazy cases,  
38 whereas it poorly correlated with  $N_{CCN}$  in clear case.  $N_{CCN}/N_{CN}$  was  
39 weakly related with BC both in foggy-hazy/hazy and clear cases. By  
40 using a simplified particle hygroscopicity ( $\kappa$ ), the calculated critical dry  
41 size (CDS) of activated aerosol did not exceed 130 nm at 0.2% SS in  
42 spite of diverse aerosol chemical compositions. The predicted  $N_{CCN}$  at  
43 0.2% SS was very successful compared with the observed  $N_{CCN}$  in clear  
44 case ( $R^2=0.96$ ) and foggy-hazy/hazy cases ( $R^2=0.91$ ). In addition, their

45 corresponding ratios of predicted to observed  $N_{CCN}$  were on average 0.95  
46 and 0.92, respectively. More organic matter is possibly responsible for  
47 this closure difference between foggy-hazy/hazy and clear cases. These  
48 results reveal that the particulate pollutant burden exerts a significant  
49 impact on  $N_{CCN}$ , especially  $N_{CCN}/N_{CN}$  promotes effectively during the  
50 polluted periods.

51

52

## 53 **1. Introduction**

54 Cloud condensation nuclei (CCN), which constitutes an important  
55 fraction of atmospheric aerosol, can influence the microphysical and  
56 radiative properties and lifetime of cloud indirectly and consequently  
57 impact the hydrological cycle (IPCC, 2013). The elevated CCN loadings  
58 ( $N_{CCN}$ ) tend to reduce cloud droplet size and then suppress precipitation  
59 in shallow and short-lived clouds (Lohmann and Feichter, 2005). But it  
60 can promote great convective overturning and enhance precipitation in  
61 deep convective clouds (Rosenfeld et al., 2008). Numerous aerosol  
62 properties, including particle size distribution, chemical composition  
63 and mixing state, are closely linked with the ability of particles to take  
64 up water vapor, i.e. the ability to act as CCN (Baumgardner et al., 2003;  
65 Kuwata and Kondo, 2008; Cubison et al., 2008). To date, the current  
66 assessment of aerosol indirect effects induced by increasing

67 anthropogenic aerosols remains poorly understood, and this brings a big  
68 uncertainty in fully picturing climate change (Andreae et al., 2005;  
69 IPCC, 2013).

70 Owing to advanced instrument development, the aerosol-cloud  
71 interaction and its impact on climate have attracted increasing attention in  
72 the last decades. Many ground-based measurements on CCN have been  
73 performed in diverse environments, describing a global map of CCN  
74 distribution in the surface atmosphere (Baumgardner et al., 2003; Yum et  
75 al., 2004, 2005; Reade et al., 2006; Juranyi et al., 2010; Leng et al., 2013).  
76 In urban environments, the new particle formation and growth, and haze  
77 pollution were observed recently as having a significant impact on  $N_{CCN}$   
78 (Ritesh et al., 2007; Kuang et al., 2009). In recent years, CCN studies  
79 have raised the relative importance of several influence factors  
80 controlling aerosol CCN activity, of which size has been announced as  
81 the major factor in determining the CCN activation of aerosol particles  
82 (Dusek et al., 2006; Anttila and Kerminen, 2007; Hudson, 2007; Quinn et  
83 al., 2008; Jimenez et al., 2009; Leng et al., 2013). However, how  
84 chemical composition especially organic compounds to link with aerosol  
85 activity and then CCN has not been fully understood. In fact, up to 90%  
86 of the aerosol population has been formed by carbonaceous substances,  
87 and among them 10-70% is water-soluble (Moffet et al., 2008; Stone et  
88 al., 2008). Particularly, various externally or internally-mixed particulate

89 components comprised in urban air mass can significantly affect the  
90 CCN-sized spectra of atmospheric particles (Svenningsson et al., 2006;  
91 Reade et al., 2006; Kuwata et al., 2007). This has posed a major challenge  
92 to study aerosol composition and predict CCN activity (Hagler et al.,  
93 2007; Hings et al., 2008; Henning et al., 2010).

94 Due to rapid industrialization in Asia for decades, anthropogenic  
95 particles and relevant precursor emissions have increased significantly,  
96 and numerous studies have indicated that the increasing anthropogenic  
97 aerosol loading has significantly changed cloud microphysical and  
98 radiative properties (Streets et al., 2000, 2008; Shao et al., 2006; Wang et  
99 al., 2006; Qian et al., 2006; Rosenfeld et al., 2007; Matsui et al., 2010;  
100 Zhang et al., 2013). In China, studies on CCN have been done widely  
101 such as at polluted sites located in Yufa (Wiedensohler et al., 2009),  
102 Beijing (Yue et al., 2011), Shouxian (Liu et al., 2011) and Shanghai (Leng  
103 et al., 2013), and suburban sites in Guangzhou (Rose et al., 2010, 2011)  
104 and Wuqing (Deng et al., 2011). To our knowledge, little attention has  
105 been paid on the impacts of fog or haze on CCN and activated aerosol  
106 particles. The increases of haze occurrences are evident in the eastern and  
107 southwestern cities in China (Che et al., 2009). Shanghai is a huge  
108 metropolis in China, and the occurrence intensity of foggy and hazy days  
109 on annual time scale has been increasing gradually especially in winter  
110 (Tie and Cao, 2009), which is deeply affected by fine particle pollution

111 enhancement and possibly linked with particle hygroscopicity (Ye et al.,  
112 2011).

113 This study presents continuous measurements of CCN and aerosol  
114 during a fog-haze episode from 6 to 9 November 2010 in Shanghai. The  
115 aim is to provide insights on CCN and aerosol activity variations under  
116 fog-haze co-occurring conditions. The instrumentation and data used in  
117 the study are described in section 2. The aerosol physical and chemical  
118 properties are introduced in section 3. Section 4 presents the evolution of  
119 CCN and aerosol activity. The relationship between aerosol and CCN is  
120 discussed in section 5. Conclusions from the study are given in section 6.

## 121 **2. Methods**

### 122 **2.1 Observational Site**

123 The instruments for CCN and aerosol measurements have been  
124 mounted roughly 20 m above ground on the roof of a building in the  
125 campus of Fudan University in Shanghai (31°18'N, 121°29'E) since  
126 October 2010. The site is surrounded by populated residential and  
127 commercial areas, as well as urban streets. The East China Sea is roughly  
128 40 km east of the site, and the prevailing wind directions are  
129 southeasterly in summer and northeasterly in winter. Local time (LT)  
130 hereafter employed in this study is 8h ahead of UTC.

### 131 **2.2 Measurements and Methodology**

132  $N_{\text{CCN}}$  was measured using a continuous flow and single column CCN

133 counter (model CCN-100, Droplet Measurement Technologies, USA), in  
134 which an optical particle counter (OPC, 0.75-10 $\mu$ m) is employed to  
135 detect activated cloud droplets (Roberts and Nenes, 2005; Lance et al.,  
136 2006). The instrument was housed in an air-conditioned weather-proof  
137 container with temperature maintaining at 20°C. The ambient aerosol  
138 airflow passed through a dryer (active carbon) to lower relative humidity  
139 below 30% before entering the instrument (Leng et al., 2013). The CCN  
140 counter was calibrated using ammonium sulfate before the study, as did  
141 calibrations for temperature gradient, flow, pressure and OPC to maintain  
142 stable SS according to the DMT operation manual. In order to ensure  
143 accurately counting, zero checks were performed before and after the  
144 campaign and regularly every two months. The effective water vapor  
145 supersaturation (SS) changed alternately at 0.2% interval within 0.2-1.0%.  
146 In real atmosphere, SS varies from slightly less than 0.1% in polluted  
147 conditions to over 1.0% in clean-air stratus cloud (Hudson and Noble,  
148 2014). The selection of SS 0.2% in the present study would benefit to the  
149 measurements in the urban environment for further analysis. Although the  
150 CCN counter can operate well under conditions of particles only in a few  
151 thousand number per cubic centimeter and corrections must need for  
152 larger concentrations ( $>5000\text{cm}^{-3}$ ) (Latham and Nenes., 2011), we still  
153 used the measured  $N_{\text{CCN}}$  directly at 0.2% SS in this study since it seldom  
154 reached the upper limit.

155 A high-resolution wide-range particle spectrometer (WPS-1000 XP,  
156 MSP) was employed to observe particle size distributions in the size  
157 range of 10 nm-10  $\mu\text{m}$ . The principles of the instrument, which have been  
158 introduced in detail by Gao et al (2009), combine the Laser Light  
159 Scattering (LPS), Condensation Particle Counting (CPC) and Differential  
160 Mobility Analysis (DMA). The DMA and CPC can effectively measure  
161 aerosol particles distributed in the size range of 10-500 nm in up to 96  
162 channels. The LPS scan the size range of 350-10,000 nm in 24 additional  
163 channels. In the present study 60 channels in DMA and 24 channels in  
164 LPS for the sample mode were chosen and 3 minutes were needed to scan  
165 the entire size range completely, as it took 2 seconds for scanning each  
166 channel. DMA was calibrated with NIST SRM 1691 and SRM 1963 PSL  
167 spheres (mean diameter of 0.269 and 0.1007  $\mu\text{m}$ , respectively) to  
168 maintain DMA transfer function properly and accurate particle sizing  
169 traceable to NIST. Four NIST traceable sizes of PSL (i.e. 0.701, 1.36, 1.6  
170 and 4.0  $\mu\text{m}$ ) were used to calculate LPS. The calibration and operating  
171 methodology of WPS has been described elsewhere (Zhang et al., 2010).  
172 In addition, we have compared the aerosol size spectra measured by WPS  
173 with those measured in parallel by a calibrated scanning mobility particle  
174 sizer (SMPS, TSI 3080) with higher accuracy in the size range of 20-800  
175 nm, including size-resolved particle concentrations and peak sizes, and a  
176 strong correlation between them was derived with correlation coefficient



177  $R^2 > 0.95$  (Leng et al., 2013). The result confirms the reliability of WPS  
178 measurements for successfully characterizing the number concentration  
179 and size distribution of condensation nuclei (CN).

180 Planetary boundary layer (PBL) height and aerosol vertical  
181 extinction profile were measured using a set of micro pulse lidar (MPL)  
182 system (MPL-4B-532) with pulse energy 6-10  $\mu\text{J}$  and pulse repetition  
183 frequency 2500 Hz. The MPL is an eye safe, compact and autonomous  
184 instrument, and an effective tool used widely in the world to provide  
185 available high spatial (30 m) and temporal resolution (30 s) information  
186 of aerosol vertical distributions (Menut et al. 1999; Cohn and Angevine,  
187 2000; Brooks, 2003). The range of lidar is roughly 30 km at night and 10  
188 km during the daytime. The description of the retrieval of aerosol  
189 parameters by the MPL will be only briefly summarized here as it has  
190 been given by He et al (2006). The vertical profile of the aerosol  
191 extinction coefficient is determined by a near end approach in solving the  
192 lidar equation (Fernald, 1984). The PBL height is determined by the MPL  
193 lidar at the altitude where a sudden decrease of scattering coefficient  
194 occurs (Boers and Eloranta, 1986). The overlap problem must be solved  
195 because it can lead to an underestimation of aerosol backscatter and  
196 extinction coefficients in the lowest altitudes having the majority of  
197 aerosols (He et al., 2006a). Outlined by Campbell et al (2002), overlap is  
198 typically solved experimentally. The system is set to point horizontally to

199 an averaged data sample with no obscuration, such as the late afternoon,  
200 when the atmosphere is well mixed and the aerosol loading is low. The  
201 backscattering over the target layer is roughly assumed constant. The  
202 similar calibration performed in 2009 showed the full overlap of about 4  
203 km and data are needed to be corrected by the overlap correction function.  
204 Welton et al (2002) fully discussed the uncertainties caused by the  
205 overlap correction and He et al (2006) estimated it to be less than 10%.

206 An online Aethalometer (AE-31, Magee Scientific Co., Berkeley,  
207 California, USA) was employed to measure black carbon (BC) at a 5-min  
208 time resolution. The instrument was operated at an airflow rate of 5 l/min.  
209 Based on the strong absorptivity of BC to light at near infrared  
210 wavelengths (Hansen et al., 1984; Weingartner et al., 2003), BC  
211 concentration is determined using the measured light attenuation at 880  
212 nm and the appropriate value of specific attenuation cross section  
213 proportional to BC mass (Petzold et al., 1997). The attenuation can be  
214 obtained by calculating the difference between light transmission through  
215 the particle-laden sample spot and the particle-free reference spot in the  
216 filter (Cheng et al., 2006; Dumka et al., 2010). The operation, calibration  
217 and maintenance of AE-31 have been described in detail by Cheng et al.  
218 (2010).

219 An online analyzer for Monitoring Aerosols and Gases (MARGA,  
220 ADI 2080, Netherlands) was employed to measure the concentration of

221 major inorganic water-soluble ions (e.g. Na<sup>+</sup>, K<sup>+</sup>, Mg<sup>+</sup>, Ca<sup>+</sup>, SO<sub>4</sub><sup>2-</sup>, Cl<sup>-</sup>,  
222 NO<sub>3</sub><sup>-</sup> and NH<sub>4</sub><sup>+</sup>) in ambient aerosol particles at 1-hour time resolution. An  
223 air pump controlled by a Mass Flow Controller (MFC) draws ambient air  
224 with airflow of 1 m<sup>3</sup>/hour into the Sample Box. An internal calibration  
225 method by using bromide for the anion chromatograph and lithium for the  
226 cation chromatograph was operated over the entire measurement period  
227 to ensure this instrument to identify and measure ion species successfully.  
228 Instructions for the methods of sampling, operation and internal  
229 calibration have been described in detail elsewhere (Du et al., 2011).  
230 Moreover, the mass concentrations of particulate matter (PM) with  
231 aerodynamic diameter less than 2.5 μm (PM<sub>2.5</sub>), meteorological factors  
232 and atmospheric visibility were measured by a continuous PM ambient  
233 monitor (FH62C14, Thermo), an automatic weather monitoring system  
234 (HydroMet<sup>TM</sup>, Vaisala) and a automatic visibility monitor at 5-min time  
235 resolution, respectively.

### 236 **2.3 Air Mass Backward Trajectory**

237 The HYSPLIT-4 model developed by the Air Resources Laboratory  
238 (ARL) of the National Oceanic and Atmospheric Administration (NOAA),  
239 USA (Draxler et al., 2003), was employed to compute 24h air mass  
240 backward trajectories ending at 500m height (AGL) and starting at 0:00  
241 LT and 12:00 LT for each day. By doing so, we can identify aerosols from  
242 different source regions and analyze their effects on aerosol activity to

243 compile a full view of the relation between fog-haze event and  $N_{CCN}$ .  
244 According to these calculated trajectories plotted in Figure 1, aerosol was  
245 classified into two categories: (1) maritime aerosol transported by air  
246 masses from marine areas on 6 Nov. 2010 carrying dominant oceanic  
247 particles, (2) continental aerosol in air mass traveling a long distance over  
248 inland areas on 7, 8 and 9 Nov. 2010 and carrying more anthropogenic  
249 particles (e.g. BC). Exactly, the maritime air mass originated from the  
250 China Eastern Sea, traveled northwesterly slow-moving across the  
251 Hangzhou Bay and finally arrived in Shanghai on 6 November. Then the  
252 air mass changed its pathway to southeasterly at around 12:00 am on 7  
253 November, and originated from northern inland areas and traveled across  
254 the North China Plain (NCP) and the eastern region of China. The  
255 continental sources contained increasing industrial and agricultural  
256 emissions (e.g. biomass burning) due to long-term rapid economy growth  
257 and large population in the last few decades. We hope to better  
258 understand the impact of aerosols with or with less anthropogenic  
259 particulate pollutants on CCN in this study by comparing these two  
260 categories.

## 261 **3. Results**

### 262 **3.1 Overview of the Fog-haze Event**

263 Haze is traditionally defined as an atmospheric phenomenon that the  
264 sky clarity is obscured by dust, smoke and other dry particles, and

265 atmospheric visibility and relative humidity (RH) are usually less than 10  
266 km and 80% over one haze episode (Fu et al., 2008). The high frequency  
267 of haze or hazy days is observed in winter, especially in the urban  
268 environments of northern China (Sun et al., 2006). During the haze event,  
269 the enhancement of particulate pollutants may greatly affect aerosol  
270 activity and  $N_{CCN}$ . The study performed in the Indo-Gangetic plain shows  
271 that winter haze exerts a significant impact on the fog and low-cloud  
272 formation (Gautam et al., 2007). Fog can be viewed as a  
273 lower-atmospheric near-surface cloud, and plays an important role in  
274 processing aerosol particles and trace gases (Gultepe et al., 2007; Biswas  
275 et al., 2008). On one hand, physically similar to cloud droplet, fog droplet  
276 also forms by water vapor condensing on dry aerosol particle under  
277 supersaturated conditions. On the other hand, generally formed in the  
278 shallow boundary layer containing local emissions, urban fog traps more  
279 pollutants than cloud at high altitudes (Fisak et al., 2002; Herckes et al.,  
280 2007). The fog or foggy case is defined as a weather with patterns of low  
281 visibility (<10 km) and higher RH (>90%). When 80% <RH< 90%, the  
282 weather was referred as a complex of haze and fog co-occurring (e.g.  
283 foggy-hazy) in the present study. Figure 2 and 3 show a 4-day time series  
284 of pressure, atmospheric visibility, RH, temperature, wind speed and  
285 direction, and PBL height from 6 to 9 November 2010. In fact, since RH  
286 seldom reached up to 90%, thus the period focused in the present study

287 were characterized as hazy and foggy-hazy cases. The haze pollution  
288 lasting at least 4 hours has been identified as one haze event by an earlier  
289 study in Shanghai, where authors paid attention to the formation of haze  
290 pollution (Du et al., 2011).

291 As shown in Figure 2-8, the 4-day period was classified into three parts:  
292 a hazy episode (marked in black open boxes) from 22:00 to 23:00 LT on 6  
293 Nov. and 10:00 LT on 7 Nov. to 13:00 LT on 8 Nov., a foggy-hazy  
294 episode (marked in red open boxes) from 23:00 LT on 6 Nov. to 10:00 LT  
295 on 7 Nov., and the rest for clear case. Statistics for meteorological  
296 conditions is listed in Table 1 where the extinction profiles are averaged  
297 for a certain altitude of 500 m. During the hazy and foggy-hazy case, the  
298 average atmospheric visibility was about 4.44 km and 2.33 km,  
299 respectively, much lower than 15.4 km in the clear case. The winds from  
300 the east and the south brought clean maritime aerosol during the clear  
301 case, however, the winds from the north and the west brought polluted  
302 anthropogenic aerosol during the hazy and foggy-hazy cases. The  
303 particulate and gaseous matters, including pollutants (e.g. BC) emitted  
304 from agricultural biomass burning were transported along the air mass  
305 pathways (Figure 1), led to a significant enhancement of aerosol  
306 extinction coefficient from hourly averages of 0.5 to 1.2 km<sup>-1</sup> (Figure 3).  
307 In addition, the PBL height downed to below 500 m and further  
308 suppressed the dilution of pollutants.

### 309 **3.2 Physical and Chemical Properties of Aerosol**

310 In order to visually identify aerosol evolution, particles in the size  
311 range of 10 nm to 10  $\mu\text{m}$  were categorized into 7 sub-size bins: 10-20 nm  
312 (nucleation mode), 20-50nm and 50-100nm (Aitken mode), 100-200nm,  
313 200-500nm and 0.5-1  $\mu\text{m}$  (accumulation mode), and 1-10  $\mu\text{m}$  (coarse  
314 mode) (Figure 4). The similar classification has been done in the  
315 measurements at the same site by Zhang et al (2010). In this study, the  
316 integrated particle size-resolved number concentrations ( $N_{\text{CN}}$ ) exhibited a  
317 regular diurnal cycle, with two peaks (9,000-16,000  $\text{cm}^{-3}$ ) almost within  
318 the traffic rush hours. The mean  $N_{\text{CN}}$  exhibited no obvious difference  
319 between the foggy-hazy (8,367  $\text{cm}^{-3}$ ) and clear (8,956  $\text{cm}^{-3}$ ) cases, but it  
320 showed a higher value (10,500  $\text{cm}^{-3}$ ) in the hazy cases, revealing a larger  
321 loading of particulate pollutants.

322 In general, the 20-100 nm (Aitken mode) particles are mostly  
323 dominant in all size particles probably due to local traffic emissions and  
324 meteorological conditions (Ferin e al., 1990). The temporal variation  
325 trend of Aitken mode was similar to  $N_{\text{CN}}$ . It was interesting that the  
326 particles of 100-500 nm (accumulation mode) dominated in  $N_{\text{CN}}$  in the  
327 hazy case with peak concentrations higher than 7,500  $\text{cm}^{-3}$ , almost twice  
328 as much as the clear case (4,000  $\text{cm}^{-3}$ ). However, the foggy-hazy case is  
329 comparable to the clear case, showing a mostly unchanged evolution of  
330 the fractions of individual size bin to total particles and  $N_{\text{CN}}$ . In addition,

331 Figure 5 shows the average size distributions (10 nm-1  $\mu\text{m}$ ) for all the  
332 three cases. It is very visible that it contains relatively more large-sized  
333 (e.g. 100 nm) aerosol particles in the aerosol population during the hazy  
334 case than that during the clear and foggy-hazy cases. Especially aerosol  
335 particles larger than 200 nm (a typical CCN size at SS 0.2%) were  
336 significantly enhanced.

337 Figure 6 shows the temporal variations of eight major inorganic water  
338 soluble ions in aerosol particles and four gaseous pollutants sampled  
339 during this study period. Measurements for  $\text{SO}_4^{2-}$ ,  $\text{Cl}^-$  and  $\text{NO}_3^-$  were  
340 unavailable from 10:00 LT on 7 Nov. to 8:00 LT on 8 Nov. Substantially,  
341 the average concentration of aerosol total water soluble ions (TWSI) in  
342 the hazy case ( $54.52 \mu\text{g m}^{-3}$ ) was comparable to the foggy-hazy case  
343 ( $50.37 \mu\text{g m}^{-3}$ ), and roughly 2 times that of the clear case ( $26.22 \mu\text{g m}^{-3}$ ).  
344 For the percentage of individual ions in TWSI,  $\text{NH}_4^+$  and  $\text{K}^+$  were  
345 relatively higher by a factor of 1.8 in the hazy and foggy-hazy cases than  
346 in the clear case. Despite the lack of  $\text{SO}_4^{2-}$  and  $\text{NO}_3^-$  partly during the  
347 hazy case, we can still conjecture their promotion on the basis of their  
348 gaseous precursor evolution of  $\text{SO}_2$  and  $\text{NO}_2$ .

349 Gaseous pollutants are released into the atmosphere from natural and  
350 anthropogenic emissions. Among them,  $\text{SO}_2$  is known as one of the most  
351 important gaseous pollutants and a precursor responsible for acid rain.  
352 Also, it can participate in the formation of new particles through



353 converting into gaseous  $\text{H}_2\text{SO}_4$ , which is the most common nucleation  
354 species due to its low vapor pressure at typical atmospheric temperature  
355 (Zhang et al., 2006b; Urone et al., 1968). Secondary aerosols produced  
356 from the formation of new particles contribute more to the global aerosol  
357 burden than primary aerosols and are important sources of CCN  
358 (Merikanto et al., 2009; Yu et al., 2008). Recent studies have shown the  
359 enhanced solubility of  $\text{SO}_2$  due to its reaction in fog droplets during a  
360 severe fog measured in the North China Plain, and this finding has  
361 provided important support for better understanding of the acidity in  
362 clouds (Zhang et al., 2013).  $\text{NO}_2$  mainly comes from vehicle traffic  
363 emissions in urban areas (Wang et al., 2006). Nitrogen oxides ( $\text{NO}$ ,  $\text{NO}_2$ ,  
364  $\text{N}_2\text{O}_5$ ) undergo heterogeneous reactions with aerosol particles (e.g. sea  
365 salt or dust) during they are transported in the atmosphere (Elizabeth et  
366 al., 2006). Thus, high gaseous pollutant content can result in larger CN  
367 loadings and subsequently more CCN particles in the atmosphere. On the  
368 whole, the loading of these precursor gases in the foggy-hazy and hazy  
369 cases exceeded that in the clear case, specifically  $\text{NO}_2$  by a factor of 2 and  
370  $\text{SO}_2$  by a factor of 1.5. Moreover,  $\text{SO}_2$  and  $\text{NO}_2$  concentrations reached  
371 their peaks around 0:00 LT on 8 November corresponding to the highest  
372 levels of CCN and aerosol activity, implying their potential effects on  
373 CCN production, which will be discussed in the next section.

### 374 **3.3. CCN Concentration and Aerosol Activity**

### 375 3.3.1 CCN and Aerosol Activity

376 Figure 7 presents the temporal variations of  $N_{CCN}$  and activated  
377 aerosol fraction ( $N_{CCN}/N_{CN}$ ) at SS 0.2%,  $N_{CN}$ , and BC during the  
378 campaign. Totally,  $N_{CN}$  fell in the range of 4,270-15,771  $\text{cm}^{-3}$  and  
379 averaged at 9,344  $\text{cm}^{-3}$ , and  $N_{CCN}$  varied between 994  $\text{cm}^{-3}$  and 6,268  $\text{cm}^{-3}$   
380 and averaged at 2,929  $\text{cm}^{-3}$ . High  $N_{CCN}/N_{CN}$  (0.41) and  $N_{CCN}$  (4,362  $\text{cm}^{-3}$ )  
381 were observed during the hazy case, followed by the foggy-hazy (0.29,  
382 2,377  $\text{cm}^{-3}$ ) and clear (0.28, 2,432  $\text{cm}^{-3}$ ) cases (Table 2). The temporal  
383 variation of  $N_{CCN}/N_{CN}$  and  $N_{CCN}$  was closely related with aerosol  
384 particle size spectra and chemical composition such as accumulation  
385 mode (100-500 nm) and water soluble ion content (Figure 4 and 6).  
386 Figure 8 gives the temporal variations of number concentrations of larger  
387 aerosol particles (e.g. particles larger than 80 nm and 100 nm) and their  
388 corresponding ratios with  $N_{CCN}$  at SS 0.2%. The larger aerosol particles  
389 showed significant increase during the hazy case and varied strongly  
390 correlated with  $N_{CCN}$ . More fractions of particles larger than 80 nm were  
391 activated into CCN during the hazy case (86%) and foggy-hazy case  
392 (84%) than that during the clear case (76%).

393 Although in different SS conditions,  $N_{CCN}$  was measured at other urban  
394 or urban-like environments such as the west coast of Tasmania (32  $\text{cm}^{-3}$ )  
395 and the west coast of Korea (5,292  $\text{cm}^{-3}$ ) at SS 1.0% (Yum et al., 2004,  
396 2005), and Mexico city (3,000  $\text{cm}^{-3}$ ), Ireland (208-346  $\text{cm}^{-3}$ ) and Vienna

397 (820  $\text{cm}^{-3}$ ) at SS 0.5% (Baumgardner et al., 2003; Reade et al., 2006;  
398 Burkart et al., 2011). An even larger  $N_{\text{CCN}}$  (6,000  $\text{cm}^{-3}$ ) was measured at  
399 SS 0.17% in Beijing (Deng et al., 2011). The average  $N_{\text{CCN}}/N_{\text{CN}}$  of this  
400 study (0.32) was higher than that measured in Vienna (0.13 at SS 0.5%,  
401 CN 13-929 nm) and Finland (0.1-0.3 at SS 0.2%, CN 3-1000 nm). The  
402 increased  $N_{\text{CCN}}/N_{\text{CN}}$  was derived at larger SS in urban environments such  
403 as Shanghai (0.47 at SS 0.8%, CN 10-10,000 nm) and Korea (0.64 at SS  
404 1.0%, CN 10-500 nm) (Yum et al., 2005; Burkart et al., 2011; Sihto et al.,  
405 2011; Leng et al., 2013).

406 As expected,  $N_{\text{CN}}$  behaved in diurnal cycle with an apparent pattern of  
407 bi-modal distribution, and  $N_{\text{CCN}}$  showed a similar temporal variation  
408 (Figure 7).  $N_{\text{CN}}$  and BC usually peaked, and reached their highest values  
409 of 15,000  $\text{cm}^{-3}$  and 35  $\mu\text{g m}^{-3}$  during the rush hours (i.e. 7:00-9:00 and  
410 16:00-19:00 LT), indicating that the anthropogenic pollutants emitted  
411 from vehicles contributes to a large part of CN and BC loadings. In  
412 addition, the favorable meteorological conditions such as low wind speed,  
413 temperature and planetary boundary layer (PBL) height also posed a great  
414 influence on  $\text{PM}_{2.5}$  and BC loadings (Figure 3). For example, the low  
415 wind speed (about 2  $\text{m s}^{-1}$ ) and PBL height (around 0.5 km) favored the  
416 mass accumulations of  $\text{PM}_{2.5}$  and BC reaching their maximums of 242  
417 and 35  $\mu\text{g m}^{-1}$  at 0:00 on 8 Nov. The later disappearance of the haze  
418 pollution was mostly owing to the wind speed increasing to 6  $\text{m s}^{-1}$  and

419 the PBL height rising to 1.4 km (Figure 2). Temperature is known as a  
420 large factor influencing PBL height and thereby indirectly impacts PM<sub>2.5</sub>  
421 and BC. In addition, the wind was frequently northwest direction and  
422 brought large amount of anthropogenic particles (e.g. BC) to Shanghai  
423 during the foggy-hazy/hazy cases, while it blew from easterly or  
424 northeasterly (marine area) before and after the polluted cases (Figure 1,  
425 2 and 7).

426 In a broad view, N<sub>CCN</sub> showed a sharp increase starting at 0:00 LT on 8  
427 Nov., and rose from 994 cm<sup>-3</sup> to 6268 cm<sup>-3</sup> within less than 10 hours.  
428 Similar to N<sub>CCN</sub>, BC also rose from 10 μg m<sup>-3</sup> to 35 μg m<sup>-3</sup> during the  
429 same period. N<sub>CN</sub> was consistent with N<sub>CCN</sub>, and they varied almost  
430 synchronously. However, N<sub>CCN</sub>/N<sub>CN</sub> changed in one step mostly opposite  
431 to N<sub>CCN</sub> and N<sub>CN</sub> (Figure 7). The possible reason for this contradictory  
432 tendency of N<sub>CN</sub> enhancement vs. N<sub>CCN</sub>/N<sub>CN</sub> reduction is that the  
433 unactivated nanoparticles, which burst partly from primary emissions of  
434 vehicles and/or partly from secondary particles due to the chemical  
435 reactions of atmospheric gaseous precursors (Figure 5) (Du et al., 2011),  
436 contributes relatively larger to N<sub>CN</sub> other than N<sub>CCN</sub>.

### 437 **3.3.2 Black Carbon and CCN**

438 As a part of hydrophobic aerosols, pure BC particles acquire  
439 hydrophilic coatings as they age in the atmosphere, and then the aged BC  
440 becomes sufficiently hydrophilic and serves as CCN for cloud

441 condensation formation (Ritesh et al., 2007). On the other hand, BC  
442 particles can release sensible heat by effectively absorbing solar radiation,  
443 thereby increasing the critical supersaturation of CCN and preventing  
444 aerosol to act as CCN (Conant et al., 2002). Biomass burning emits a  
445 large amount of trace gases and carboneous particles into the atmosphere,  
446 and leads to changes in climate and precipitation, as well as aquatic and  
447 terrestrial ecosystem (Andreae et al., 2004). The wild fires contribute a  
448 significant fraction of global CCN burden (Pierce et al., 2007; Andreae et  
449 al., 2009). Large quantities of active agricultural fire sites were detected  
450 from satellites over China on 7 November 2010 (Figure 1), whereas no  
451 obvious wild biomass burning activities were observed during the rest  
452 days. Based on the calculated 24-h air mass backward trajectories, the air  
453 mass that passed right through the agricultural fire regions in the Jiangsu  
454 and Anhui provinces on 7 November reached the sampling site in the next  
455 day, bringing large quantities of aged BC particles after a long range  
456 transport. This resulted in a severe increase of particle mass concentration  
457 and a significant enhancement of aerosol extinction coefficient on 7 and 8  
458 November (Figure 3). As discussed in section 3.2, NO<sub>2</sub> and SO<sub>2</sub>  
459 concentrations increased synchronously during the whole period (Figure  
460 6), and they would undergo heterogeneous reactions on the surface of BC  
461 particles to change particle microphysical and chemical properties,  
462 making BC particles sufficiently hydrophilic to act as CCN (Ritesh et al.,

463 2007).

464 Relationship analyses between  $N_{CCN}$ ,  $N_{CCN}/N_{CN}$  and BC were  
465 calculated using hourly-averaged data, and the correlation coefficients ( $R^2$ )  
466 are presented in Figure 9. Surprisingly, BC strongly correlated with  $N_{CCN}$   
467 ( $R^2=0.85$ ) in the foggy-hazy and hazy cases, whereas they showed a poor  
468 linear relationship ( $R^2=0.25$ ) in the clear case. The possible reason is BC  
469 particle aging by heterogeneous reactions with gaseous pollutants (e.g.  
470  $NO_2$  and  $SO_2$ ) to be activated CCN during pollutant atmospheric transport  
471 (Ritesh et al., 2007). In addition, so many studies have proposed that the  
472 aged BC is efficient CCN (Dusek. et al., 2006; Anttila and Kerminen,  
473 2007; Hudson, 2007). However,  $N_{CCN}/N_{CN}$  was poorly related with BC  
474 for both foggy-hazy/hazy and clear cases ( $R^2=0.43$  and  $0.07$ , respectively),  
475 indicating that BC maybe a relatively more important contributor to  
476 unactivated particles especially in nanoscale sizes (e.g. traffic emission)  
477 than activated CCN.

### 478 **3.4. Relationship of Aerosol and CCN**

479 Although aerosol size distributions were measured only in the size  
480 range of 10-10,000 nm, they were still used to predict  $N_{CCN}$  according to  
481 Köhler theory (Köhler et al., 1936). Toward this end, the particle  
482 hygroscopicity “kappa” ( $\kappa$ ) was used in the closure calculation. The  
483 description of the technique has been given by Petters and Kreidenweis  
484 (2007), therefore it will only be briefly summarized here. The  $\kappa$

485 parameter for one multicomponent particle can be obtained through  
486 weighting each component  $\kappa_i$  by their volume fractions in the mixture,

$$487 \quad \kappa = \sum_i \varepsilon_i \kappa_i \quad (1)$$

488 where  $\varepsilon_i$  is the volume fraction of chemical compounds in particles,  
489 and  $\kappa_i$  is the effective  $\kappa$  of individual chemical composition.

490 Assuming aerosol particles are completely internal-mixed, a simplified  
491  $\kappa$  was calculated using water soluble inorganic ions (organic matter data  
492 is unavailable). Aerosol particle compositions were classified into three  
493 categories (Petters and Kreidenweis, 2007; Wiedensohler et al., 2009),  
494 and  $\kappa_i$  and densities for each component are shown in Table 3, in which  
495 ‘others’ is defined as ‘PM<sub>2.5</sub>-BC-inorganic ions’. The critical dry size  
496 (CDS) of particle to be activated as CCN at one SS can hence be  
497 determined by the following equation:

$$498 \quad S(D) = \frac{D^3 - D_d^3}{D^3 - D_d^3(1 - \kappa)} \exp\left(\frac{4\sigma_{s/a} M_w}{RT\rho_w D}\right) \quad (2)$$

499 where  $\rho_w$  is the density of water,  $M_w$  is the molecular weight of water,  
500  $\sigma_{s/a}$  is the surface tension of the solution/air interface,  $R$  is the universal  
501 gas constant,  $\kappa$  is the hygroscopicity parameter,  $T$  is temperature,  $D_d$  is the  
502 dry diameter,  $D$  is the diameter of the droplet and  $S(D)$  is the critical dry  
503 size under a given SS. Detailed information for the derivation of equation  
504 (2) can be found in Petters and Kreidenweis (2007). Equation (2) applies  
505 over the entire range of humidity and solution hygroscopicity and can be

506 utilized to predict the conditions of cloud droplet activation. The critical  
507 SS for a selected dry size of particle is determined from the maximum of  
508 the curve for equation (2). Computed for  $\sigma_{s/a}=0.072 \text{ J m}^{-2}$  and  $T=298.15 \text{ K}$ ,  
509 the calculated CDS varied between 60 nm and 130 nm and averaged at  
510 102 nm. Particularly, the hourly-averaged CDS during the  
511 foggy-hazy/hazy cases was slightly lower (96 nm) than during the clear  
512 case (105 nm). So far, the comparable or relatively higher CDS has also  
513 been found in diverse regions and for various aerosol types, despite of  
514 different calculation models and SS. For example, the fresh aerosol  
515 particles emitted by an aircraft internal combustion engine have a CDS  
516 range of 146-301 nm at SS 0.7%, depending on varying operating  
517 conditions (Hitzenberger et al., 2003). Furutani et al (2008) investigated  
518 three types of aerosol masses along the southern coast of California, and  
519 the CDS was estimated at 110 nm at SS 0.6% for fresh ship exhaust,  
520 70-110 nm for fresh anthropogenic aerosols and roughly 50 nm for aged  
521 anthropogenic and clean maritime aerosols. In Vienna, the CDS has a  
522 wide gap between 69 nm and 368 nm, and averaged at 169 nm (Burkart et  
523 al., 2011). Quinn et al (2008) observed the CDS in a narrow range of 70-  
524 90 nm for maritime aerosols in the Gulf of Mexico, and a moderate range  
525 of 90-170 nm in the ship channels of Houston with high marine traffic  
526 densities close to industrial and anthropogenic sources.

527 The CCN population can be effectively viewed as a subset of measured



528 aerosol size distributions since the operating range (10-10,000 nm)  
529 includes the majority of atmospheric particles. Therefore, the predicted  
530  $N_{CCN}$  can be calculated through integrating particles upward in size from  
531 the bottom CDS to the upper boundary. In this calculation, the predicted  
532  $N_{CCN}$  of hourly-averaged were compared with the measured ones  
533 correspondingly.

534 The results of this closure analysis are shown in scatterplot in Figure  
535 10 and 11. The prediction for CCN is generally success throughout the  
536 entire data set. The linear regression between predicted and measured  
537  $N_{CCN}$  produces a slope of 1.012 and an intercept of  $128.3 \text{ cm}^{-3}$  ( $R^2=0.95$ ),  
538 and the average ratio of predicted versus measured  $N_{CCN}$  is 0.94 (Figure  
539 10). The results indicate some moderate underestimate (about 6% on  
540 average) but the agreement is still excellent. The achieved closure  
541 calculation suggested that water soluble inorganic ions played a major  
542 role in contributing the  $\kappa$  value. In fact, 83.8% of the  $\kappa$  was expressed  
543 by  $\text{SO}_4^{2-} + \text{NO}_3^- + \text{NH}_4^+$  in total (in another study by our group, not  
544 published yet), with their individual contribution to be 39.8%, 31.7%  
545 and 12.3%, respectively. In addition, it is worth note that the predicted  
546  $N_{CCN}$  at SS 0.2% was more correlated with the observed  $N_{CCN}$  in the clear  
547 case ( $R^2=0.96$ ) than the foggy-hazy/hazy cases ( $R^2=0.91$ ), and the  
548 corresponding ratios of predicted to observed  $N_{CCN}$  were 0.95 and 0.92,  
549 respectively (Figure 11). In all cases, the mean ratio of predicted to

550 observed  $N_{CCN}$  never reached up to 1, suggesting that organic matter  
551 would play a second role and make up the rest of  $\kappa$ .

#### 552 **4. Conclusions and discussion**

553 A continuous 4-day data obtained at an urban site of Shanghai over a  
554 fog-haze event from 6 to 9 November 2012 was analyzed for CCN and  
555 aerosol. Overall, meteorological conditions such as wind speed, wind  
556 direction and temperature exerted a great influence on  $PM_{2.5}$  and BC  
557 loadings. Human activity is an essential factor to control emissions of  
558 aerosol and CCN in urban environments.  $N_{CCN}/N_{CN}$  and  $N_{CCN}$  usually  
559 were higher in the hazy case due to increased aerosols in the  
560 accumulation mode, and lower in the foggy-hazy and clear cases.  
561 DeFelice et al (1996) also found the reduction of CCN concentration  
562 under foggy and rainy conditions in the Antarctic area. Of special interest,  
563 the low  $N_{CCN}/N_{CN}$ ,  $N_{CN}$  and  $N_{CCN}$  during the foggy-hazy case can  
564 plausibly explain in three aspects: (1) the limited data input introduces  
565 some uncertainties, (2) the possible physical effects such as boundary  
566 layer evolution, transportation and atmospheric dilution are not  
567 considered, (3) the plausible emergence of fog droplets and particles  
568 leads to the reduction of aerosol number concentration.

569 BC was correlated well with  $N_{CCN}$  in the foggy-hazy and hazy cases,  
570 while they were less linked in the clear case. Besides, there were no good  
571 agreements between BC and  $N_{CCN}/N_{CN}$ , with moderate ( $R^2=0.43$ ) and

572 poor ( $R^2=0.07$ ) correlation coefficients for the foggy-hazy/hazy cases and  
573 clear case, respectively. More BC is aged during the foggy-hazy/hazy  
574 cases, hence more CCN is activated (Dusek et al., 2006; Anttila and  
575 Kerminen., 2007; Hudson., 2007). However, there exists a different  
576 perspective. For example, BC has been found to significantly suppress  
577 cloud formation in the Indo-Gangetic plain (Ritesh et al., 2007). Pure BC  
578 particles are hydrophobic and can release heat by absorbing solar  
579 radiation, hence they would increase the critical SS of aerosol to act as  
580 CCN and further suppress the tendency of CCN to become cloud droplets.  
581 However, aged BC particles are sufficiently hydrophilic by acquiring  
582 hydrophilic coatings in the atmosphere, and become CCN and favor  
583 aerosol indirect forcing (Conant et al., 2002; Ritesh et al., 2007). In this  
584 study, BC particles moved a long-distance from inland and aged during  
585 the transporting process, thereby it favors CCN formation.

586 By using a simplified  $\kappa$  parameter, the critical dry size never exceeded  
587 130 nm. In spite of the absence of organic matter, the CCN closure  
588 calculation was still achieved, suggesting that aerosol major water soluble  
589 ions contribute to effective  $\kappa$ . The predicted  $N_{CCN}$  was close to the  
590 observed during the clear case than the foggy-hazy/hazy cases  
591 having more organic matter. In summary, water soluble inorganic  
592 ions constituted the majority of particle hygroscopicity ( $\kappa$ ) estimation,  
593 while organic matter made up the rest. It is noted that organic matter is

594 essential to build the exact CCN prediction models.

595 This paper mainly explored how  $N_{CCN}$ ,  $N_{CN}$  and  $N_{CCN}/N_{CN}$  vary under a  
596 fog-haze co-occurring condition, as well as the major influential factors  
597 to these activities. The results revealed that the particulate pollutant  
598 burden exerts a significant impact on  $N_{CCN}$ , especially  $N_{CCN}/N_{CN}$  is  
599 effectively promoted during the polluted periods (e.g. haze). Importantly,  
600 the fog-haze transformation is highly complicated involving numerous  
601 changes of aerosol in physical and chemical properties, which remains  
602 poorly understood. The clear and hazy cases both continued more than  
603 one day with a reduced effect of diurnal variation. Foggy conditions  
604 mostly occur at night and in the morning and seldom last as long as 24  
605 hours in Shanghai, thereby it was inevitable that the diurnal variations  
606 had some effect on the results during the foggy-hazy case spanning from  
607 23:00 LT on 6 Nov. to 10:00 LT on 7 Nov.. There presents the results of  
608 only a case, so more efforts are needed for highlighting the  
609 comprehensive effects of fog and haze on CCN in urban environments.

610

## 611 **Acknowledgements**

612 This research is supported by the National Basic Research Program of  
613 China (2010CB428503), the National Natural Science Foundation of  
614 China (41075096, 21190053, 21177025, 21277028, 21377029,  
615 41475109), and partly by the Research and Development Special Fund

616 for Public Welfare Industry (Meteorology) of CMA (GYHY201006047),  
617 the Shanghai Science and Technology Commission of Shanghai  
618 Municipality (12DJ1400100, 12DZ2260200), the Jiangsu Collaborative  
619 Innovation Center for Climate Change, and Priority fields for Ph.D.  
620 Programs Foundation of Ministry of Education of China (0110071130003)  
621 and FP7 project (AMIS, PIRSES-GA-2011).

622

## 623 **Reference**

624 Andreae, M. O., et al.: Correlation between cloud condensation nuclei  
625 concentration and aerosol optical thickness in remote and polluted  
626 regions, *Atmos. Chem. Phys.*, 9, 543-556, doi: 10.5194/acp-9-543-2009,  
627 2009.

628 Andreae, M. O., et al.: Smoking rain clouds over the Amazon, *Science.*,  
629 303, 1337-1342, doi: 10.1126/science. 1092779,2004.

630 Andreae, M. O., Jones, C. D., and Cox. P. M.: Strong present-day aerosol  
631 cooling implies a hot future, *Nature.*, 435, 1187-1190, 2005.

632 Anttila, T., and Kerminen, V. M.: On the contribution of Aitken mode  
633 particles to cloud droplet populations at continental back-ground areas-a  
634 parametric sensitivity study, *Atmos. Chem. Phys.*, 7, 4625-4637, 2007.

635 Baumgardner, D., Raga, G. B., and Muhlia, A.: Evidence for the  
636 formation of CCN by photochemical processes in Mexico City, *Atmos.*  
637 *Environ.*, doi:10.1016, 2003.

638 Biswas, K. F., Ghauri, B. M., and Husain, L.: Gaseous and aerosol  
639 pollutants during fog and clear episodes in South Asian urban  
640 atmosphere, *Atmos. Environ.*, 42, 7775-7785, 2008.

641 Boers, R., and Eloranta, E.W.: Lidar measurements of the atmospheric  
642 entrainment zone and the potential temperature jump across the top of  
643 the mixed layer, *Boundary-Layer Meteorology*, 34, 357-375, 1986.

644 Brooks, I.M.: Finding boundary layer top: application of a wavelet  
645 covariance transform to lidar backscatter profiles, *Journal of*  
646 *Atmospheric and Oceanic Technology*, 20, 1092-1105, 2003.

647 Burkar, J., Steiner, G., Reischl, G., and Hitzenberger, R.: Long-term study  
648 of cloud condensation nuclei (CCN) activation of atmospheric aerosol in  
649 Vienna, *Atmos. Environ.*, 45, 5751-5759, 2011.

650 Campbell, J.R., Hlavka, D.L., Welton, E.J., Flynn, C.J., Turner, D.D.,  
651 Spinhirne, J.D., Scott, V.S., and Hwang, I.H.: Full-time, eye-safe cloud  
652 and aerosol lidar observation at atmospheric radiation measurement  
653 program sites: Instruments and data processing, *J. Atmos. Oceanic*  
654 *Technol.*, 19, 431-442, 2002.

655 Che, H. Z., Zhang, X. Y., Li, Y., Zhou, Z. J., Qu, John. J and Hao, X. J.:  
656 Haze trends over the capital cities of 31 provinces in China, 1981-2005,  
657 *Theor. Appl. Climatol.*, 97, 235-242, 2009.

658 Cheng, T. T., Han, Z. W., Zhang, R. J., Du, H. H., Jia, X., Wang, J. J., and  
659 Yao, J. Y.: Black carbon in a continental semi-arid area of Northeast

660 China and its possible sources of fire emission, *J. Geophys. Res.*, 115,  
661 D23204, doi: 10.1029/2009JD013523, 2010.

662 Cheng, Y., Lee, S. C., Ho, K. F., Wang, Y. Q., Cao, J. J., Chow, J. C., and  
663 Watson, J. G.: Black carbon measurement in a coastal area of south  
664 China, *J. Geophys. Res.*, 111, D12310, doi: 10.1029/2005JD006663,  
665 2006.

666 Cohn, S.A., Angevine W.M.: Boundary layer height and entrainment zone  
667 thickness measured by lidars and wind-profiling radars. *Journal of*  
668 *Applied Meteorology*, 39, 1233-1247, 2000.

669 Conant, W. C., A. Netes, and J. H. Seinfeld.: Black carbon radiative  
670 heating effect on cloud microphysics and implications for the aerosol  
671 indirect effect: 1. Extended Köhler theory, *J. Geophys. Res.*, 107 (D21),  
672 4604, doi:10.1029/2002JD002094, 2002.

673 Cubison, M. J., Ervens, B., Feingold, G., Docherty, K. S., Ulbrich, I. M.,  
674 Shields, L., Prather, K., Hering, S. and Jimenez, J. L.: The influence of  
675 chemical composition and mixing state of Los Angeles urban aerosol on  
676 CCN number and cloud properties, *Atmos. Chem. Phys.*, 8, 5649-5667,  
677 2008.

678 DeFelice, T. P.: Variation in cloud condensation nuclei at Palmer station  
679 Antarctica during February 1994, *Atmos. Res.*, 41, 229-248, 1996.

680 Deng, Z. Z., Zhao, C. S., Ma, N.P., Liu, F., Ran, L., Xu, W. Y., Liang, Z.,  
681 Liang, S., Huang, M. Y., Ma, X.C., Zhang, Q., Quan, J. N., and Yan, P.:

682 Size- resolved and bulk activation properties of aerosols in the North  
683 China Plain, *Atmos. Chem. Phys.*, 11, 3835-3846, 2011.

684 Draxler, R. R., and Rolph, G. D.: HYSPLIT(Hybrid Single-Particle  
685 Lagrangian Integrated Trajectory) Model access via NOAA ARL  
686 READY Website (<http://www.arl.noaa.gov/ready/hysplit4.htm>), NOAA  
687 Air Resources Laboratory, Silver Spring, MD, 2003.

688 Du, H., Kong, L., Cheng, T., Chen, J., Du, J., et al.: Insights into  
689 summertime haze pollution events over Shanghai based on online  
690 water-soluble ionic composition of aerosols, *Atmos. Environ.*, 45,  
691 5131-5137, 2011.

692 Dumka, U.C., Krishna Moorthy, K., Rajesh Kumar, Hegde, P., Ram Sagar,  
693 Pant, P., et al.: Characteristics of aerosol black carbon mass  
694 concentration over a high altitude location in the Central Himalayas  
695 from multi-year measurements, *Atmos. Res.*, 96, 510-521, 2010.

696 Dusek, U., Frank, G. P., and Hildebrandt, L.: Size matters more than  
697 chemistry for cloud- nucleating ability of aerosol particles, *Science*, 312,  
698 1375-1378, 2006.

699 Elizabeth, R. G., Paula, K. H., and Vicki, H. G.: Physicochemical  
700 properties of nitrate aerosols: Implications for the atmosphere, *J. Phys.*  
701 *Chem.*, 110, 11785-11799, 2006.

702 Ferin, J., Oberdoerster, G., Penney, D. P., Soderholm, S. C., Gelein, R.,  
703 and Piper, H. C.: Increased pulmonary toxicity of ultrafine particles 1.



704 Particles clearance, translocation, morphology, *J. Aerosol Sci.*, 21 (3),  
705 381-384, 1990.

706 Fernald, F. G.: Analysis of atmospheric lidar observations: Some  
707 comments, *Appl. Opt.*, 23(5), 652-653, 1984.

708 Fisak, J., Tesar, M., Rezacova, D., Elias, V., Weignerova, V., and Fottova,  
709 D.: Pollutant concentrations in fog and low cloud water at selected sites  
710 of the Czech Republic, *Atmos. Res.*, 64, 75-87, 2002.

711 Fu, Q. Y., Zhuang, G. S., Wang, J., Xu, C., Huang, K., Li, J., Hou, B., Lu,  
712 T., and Streets, D. G.: Mechanism of formation of the heaviest  
713 pollution episode ever recorded in the Yangtze River Delta, China,  
714 *Atmos. Environ.*, 42, 2023-2036, 2008.

715 Furutani. H., Dall'Osto, M., Roberts, G. C., and Prather, K. A.:  
716 Assessment of the relative importance of atmospheric aging on CCN  
717 activity derived from field observations, *Atmos. Environ.*, 42,  
718 3130-3142, 2008.

719 Gao, J., Wang, T., Zhou, X. H., Wu, W. S., and Wang, W. X.:  
720 Measurement of aerosol number size distributions in the Yangtze River  
721 delta in China: formation and growth of particles under polluted  
722 conditions, *Atmos. Environ.*, 43 (4), 829-836, 2009.

723 Gautam, R., Hsu, N. C., Kafatos, M. and Tsay, S. C.: Influences of winter  
724 haze on fog/low cloud over the Indo-Gangetic plains, *J. Geophys. Res.*,  
725 112, D05207, doi: 10.1029/2005JD007036, 2007.

726 Gulpete, I., Tardif, R., Michaelides, S. C., Cermak, J., Bott, A., Bendix, J.,  
727 Müller, M. D., Pagowski, M., Hansen, B., Ellrod, G., Jacobs, W., Toth,  
728 G., and Cober, S. G.: Fog research: a review of past achievements and  
729 future perspectives, *Pure and Applied Geophys.*, 164, 1121-1159, 2007.

730 Hagler, G. S. W., Bergin, M. H., Smith, E. A. and Dibb, J. E.: A summer  
731 time series of particulate carbon in the air and snow at Summit,  
732 Greenland, *J. Geophys. Res.*, 112, D21309, doi: 10.1029/2007JD008993,  
733 2007.

734 Hansen, A. D. A., Rosen, H., and Novakov T.: The aethalometer-an  
735 instrument for the real-time measurement of optical absorption by  
736 aerosol particles, *Sci. Total Environ.*, 36, 191-196, 1984.

737 He, Q. S., Li, C. C., Mao, J. T., Lau, A. K. H., and Li, P. R.: A study on  
738 the aerosol extinction-to-backscatter ratio with combination of  
739 micro-pulse LIDAR and MODIS over Hong Kong, *Atmos. Chem. Phys.*,  
740 6, 3243-3256, 2006.

741 Henning, S., Wex, H., Hennig, T., Kiselev, A., Snider, J. R., Rose, D., et  
742 al.: Soluble mass, hygroscopic growth, and droplet activation of coated  
743 soot particles during LACIS Experiment in November (LEXNo), *J.*  
744 *Geophys. Res.*, 115, D11206, doi: 10.1029/2009JD012626, 2010.

745 Herckes, P., Chang, H., Lee, T., and Collett Jr., J. L.: Air pollution  
746 processing by radiation fogs, *Water, Air, & Soil Pollution* 181 (1), 65-75,  
747 2007.

748 Hings, S. S., Wrobel, W. C., Cross, E. S., Worsnop, D. R., Davidovits, P.  
749 and Onasch, T. B.: CCN activation experiments with adipic acid: effect  
750 of particle phase and adipic acid coatings on soluble and insoluble  
751 particles, *Atmos. Chem. Phys.*, 8, 3735-3748, 2008.

752 Hitzenberger, R., Giebl, H., Petzold, A., Gysel, M., Nyeki, S.,  
753 Weingartner, E., Baltensperger, U., and Wilson, W. C.: Properties of jet  
754 engine combustor particles during the PartEmis experiment.  
755 Hygroscopic properties at supersaturated conditions, *Geophys. Res.*  
756 *Lett.*,30 (14), 1779, doi: 10.1029/2003GL017294, 2003.

757 Hudson, J.: Variability of the relationship between particle size and  
758 cloud-nucleating ability, *Geophys. Res. Lett.*, 34, L08801, doi:  
759 10.1029/2006GL028850, 2007.

760 Hudson, J. G. and Noble, S.: CCN and vertical velocity influence on  
761 droplet concentration and supersaturations in clean and polluted stratus  
762 clouds, *J. Atmos. Sci.*, 106, 24119-24126, 2014.

763 IPCC: Climate Change 2013: The Physical Science Basis. Contribution of  
764 Working Group I to the Fifth Assessment Report of the  
765 Intergovernmental Panel on Climate Change, edited by: Jousaume, S.,  
766 Penner, J., and Tangang, F., IPCC, Stockholm, 2013.

767 Jimenez, J. L. et al.: Evolution of organic aerosols in the atmosphere,  
768 *Science*, 326, 1525-1529, 2009.

769 Juranyi, Z., Gysel, M., Weingartner, E., DeCarlo, P. F., Kammermann, L.,

770 and Balternsperger, U.: Measurement and modeled cloud condensation  
771 nuclei concentration at the high alpine site Jungfraujoch, *Atmos. Chem.*  
772 *Phys. Discussions.*, 10, 8859-8897, 2010.

773 Köhler, H.: The nucleus in and the the growth of hygroscopic droplets, *T.*  
774 *Faraday Soc.*, 32, 1152-1161, 1936.

775 Kuang, C., McMurry, P. H., and McCormick, A.V.: Determination of  
776 cloud condensation nuclei production from measured new particle  
777 formation events, *Geophys. Res. Lett.*, 36, L09822, doi: 10.  
778 1029/2009GL037584, 2009.

779 Kuwata, M. and Kondo, Y.: Dependence of size-resolved CCN spectra on  
780 the mixing state of nonvolatile cores observed in Tokyo. *J. Geophys.*  
781 *Res.*, 113, D19202, doi; 10.1029/2007JD009761, 2008.

782 Kuwata, M., Kondo, Y., Mochida, M., Takegawa, N. and Kawamura, K.:  
783 Dependence of CCN activity of less volatile particles on the amount of  
784 coating observed in Tokyo, *J. Geophys. Res.*, 112, D11207, doi:  
785 10.1029/2006JD007758, 2007.

786 Lance, S., Medina, J., Smith, J. N., and Nenes, A.: Mapping the operation  
787 of the DMT Continuous Flow CCN counter, *Aerosol Sci. Tech.*, 40,  
788 242-254, 2006.

789 Lathem, T. L., and Nenes A.: Water vapor depletion in the DMT  
790 Continuous Flow CCN Chamber: Effects on supersaturation and droplet  
791 growth, *Aerosol Sci. Tech.*, 45(5), 604-615, 2011.

792 Leng, C. P., Cheng, T. T., Chen, J. M., et al.: Measurements of surface  
793 cloud condensation nuclei and aerosol activity in downtown Shanghai,  
794 *Atmos. Environ.*, 69, 354-361, 2013.

795 Liu, J. J., Zheng, Y. F., Li, Z. Q., and Cribb, M.: Analysis of cloud  
796 condensation nuclei properties at a polluted site in southeastern China  
797 during the AMF-China Campaign, *J. Geophys. Res.*, 116, D00K35, doi:  
798 10.1029/2011JD016395, 2011.

799 Lohmann, U. and Feichter, J.: Global indirect aerosol effect; a review,  
800 *Atmos. Chem. Phys.*, 5, 715-737, 2005.

801 Matsui, H., Koike, M., Kondo, Y., Takegawa, N., Fast, J. D., Pöschl, U.,  
802 Garland, R. M., Andreae, M. O., Wiedensohler, A., Sugimoto, N., and  
803 Zhu, T.: Spatial and temporal variations of aerosols around Beijing in  
804 summer 2006: 2. Local and column aerosol optical properties, *J.*  
805 *Geophys. Res.*, 115, D22207, doi: 10.1029/2010JD013895, 2010.

806 Menut, L., Flamant, C., Pelon, J., Flamant, P. H.: Urban boundary-layer  
807 height determination from lidar measurements over the Paris area. *Appl.*  
808 *Optics.* 38, 945-954, 1999.

809 Merikanto, J., Sprackken, D. V., Mann, G. W., Pickering, S. J and Carslaw,  
810 K. S.: Impact of nucleation on global CCN, *Atmos. Chem. Phys.*, 9(21),  
811 8601-8616, 2009.

812 Moffet, R. C., de Foy, B., Molina, L. T., Molina, M. J. and Prather, A.:  
813 Measurements of ambient aerosols in northern Mexico City by single

814 particle mass spectrometry, *Atmos. Chem. Phys.*, 8, 4499-4516, 2008.

815 Petters, M. D., and S. M. Kreidenweis.: A single parameter representation  
816 of hygroscopic growth and cloud condensation nucleus activity, *Atmos.*  
817 *Chem. Phys.*, 7, 1961-1971, 2007.

818 Petzold, A., Kopp, C. and Niessner R.: The dependence of the specific  
819 attenuation cross-section on black carbon mass fraction and particle  
820 size, *Atmos. Environ.*, 31(5), 661-672, 1997.

821 Pierce, J. R., et al.: Contribution of primary carbonaceous aerosol to  
822 cloud condensation nuclei: Processes and uncertainties evaluated with  
823 a global aerosol microphysics model, *Atmos.Chem. Phys.*, 7,  
824 5447-5466, doi: 10.5194/acp-7-5447-2007, 2007.

825 Qian, Y., Kaiser, D. P., Leung, L. R., and Xu, M.: More frequent  
826 cloud-free sky and less surface solar radiation in China from 1955-2000,  
827 *Geophys. Res. Lett.*, 33, L01812, doi:10.1029/2005GL024586, 2006.

828 Quinn, P. K., Bates, T. S., Coffman, D. J. and Covert, D. S.: Influence of  
829 particle size and chemistry on the cloud nucleating properties of aerosols,  
830 *Atmos. Chem. Phys.*, 8, 1029-1042, 2008.

831 Reade, L., Jennings, S. G., and Gobnait, M.: Cloud condensation nuclei  
832 measurements at Mace Head, Ireland, over the period 1994-2002, *Atmos.*  
833 *Res.*, 82, 610-621, 2006.

834 Ritesh, G., Christina, H., Menas. Kafatos., Si-Chee. T.: Influences of  
835 winter haze on fog/low cloud over the Indo-Gangetic plains. *J. Geophys.*

836 Res., 112, D05207, doi: 10. 1029/2005JD007036, 2007.

837 Roberts, G. C. and Nenes, A.: A continuous-flow streamwise  
838 thermal-gradient CCN chamber for atmospheric measurements, *Aerosol*  
839 *Sci. Tech.*, 39, 206-221, 2005.

840 Rose, D., Gunthe, S. S., Su. H., Carland. R. M., Yang. H., et al.: Cloud  
841 condensation nuclei in polluted air and biomass burning smoke near the  
842 mega-city Guangzhou, China- Part 2: Size-resolved aerosol chemical  
843 composition, diurnal cycles, and externally mixed weakly CCN-active  
844 soot particles, *Atmos. Chem. Phys.*, 11, 2817-2836, 2011.

845 Rose, D., Nowak, A., Achtert. P., Wiedensohler. A., Hu. M., et al.: Cloud  
846 condensation nuclei in polluted air and biomass burning smoke near the  
847 mega-city Guangzhou, China- Part 1: Size-resolved measurements and  
848 implications for the modeling of aerosol particle hygroscopicity and  
849 CCN activity, *Atmos. Chem. Phys.*, 10, 3365-3383, 2010.

850 Rosenfeld, D., Dai, J., Yu, X., Yao, Z., Xu, X., Wang, X., and Du, C.:  
851 Inverse relations between amounts of air pollution and orographic  
852 precipitation, *Science*, 315, 1396-1398, 2007.

853 Rosenfeld, D., Lohmann, U., Raga, G. B., O'Dowd, C. D., Kulmala, M.,  
854 Fuzzi, S., Reissell, A., and Andreae, M. O.: Flood or Drought: How Do  
855 Aerosol Affects Precipitation?, *Science*, 321, 5894, 2008.

856 Shao, M., Tang, X., Zhang, Y., and Li, W.: City clusters in China: air and  
857 surface water pollution, *Front. Ecol. Environ*, 4, 353-361, 2006.

858 Sihto, S. L., Mikkilä, J., Vanhanen, J., et al.: Seasonal variation of CCN  
859 concentrations and aerosols activation properties in boreal forest, *Atmos.*  
860 *Chem. Phys.*, 11, 13269-13285, 2011.

861 Stone, E. A., Snyder, D. C., Sheesley, R. J., Sullivan, A. P., Weber, R. J.  
862 and Schauer, J. J.: Source apportionment of fine organic aerosol in  
863 Mexico City during the MILAGRO experiment 2006, *Atmos. Chem.*  
864 *Phys.*, 8, 1249-1259, 2008.

865 Streets, D. G., Tsia, N. Y., Akimoto, H., and Oka, K.: Sulfur dioxide  
866 emissions in Asia in the period 1985-1997, *Atmos. Environ.*, 34,  
867 4413-4424, 2000.

868 Streets, D. G., Yu, C., Wu, Y., Chin, M., Zhao, Z., Hayasaka, T., and Shi,  
869 G.: Aerosol trends over China, 1980-2000, *Atmos. Res.*, 88, 174-182,  
870 2008.

871 Sun, Y. L., Zhuang, G. S., Tang, A. H., Wang, Y., and An, Z. S.: Chemical  
872 characteristics of PM<sub>2.5</sub> in haze-fog episodes in Beijing, *Environ. Sci.*  
873 *Tech.*, 40, 3148-3155, 2006.

874 Svenningsson, B., Rissler, J., Swietlicki, E., Mircea, M., Bilde, M., et al.:  
875 Hygroscopic growth and critical supersaturations for mixed aerosol  
876 particles of inorganic and organic compounds of atmospheric relevance,  
877 *Atmos. Chem. Phys.*, 6, 1937-1952, 2006.

878 Tie, X. and Cao, J.: Aerosol pollution in China: present and future impact  
879 on environment, *Particuology.*, 7, 426-43, 20091.



880 Urone, P., Lutsep, Helmut., Noyes. C. M., and Parcher, J. F.: Static  
881 studies of sulfur dioxide reactions in air, *Environ. Sci. Tech*, 2(8),  
882 611-618, 1968.

883 Wang, Y., Zhuang, G. S., Zhang, X. Y., Huang, K., Xu, C., Tang, A. H.,  
884 Chen, J. M., and An, Z. S.: The ion chemistry, seasonal cycle, and  
885 sources of PM<sub>2.5</sub> TSP aerosol in Shanghai, *Atmos. Environ.*,40,  
886 2935-2952, 2006.

887 Weingartner, E., Saathoff, H., Schnaiter, M., Streit, N., Bitnar, B., and  
888 Baltensperger U.: Absorption of light by soot particles: determination of  
889 the absorption coefficient by means of aethalometers, *J. Aerosol Sci.*, 34,  
890 1445-1463, 2003.

891 Wiedensohler, A., Cheng, Y. F., Nowak, A., Wehner. B., Achtert, P.,  
892 Berghof, M., Birmili, W., Wu, Z. J., et al.: Rapid aerosol growth and  
893 increase of cloud condensation nucleus activity by secondary aerosol  
894 formation and condensation: A case study for regional air pollution in  
895 northeastern China, *Geophys. Res. Lett.*,114, D00G08, doi:  
896 10.1029/2008JD010884, 2009.

897 Ye, X. N., Ma, Z., Zhang, J. C., Du, H. H., Chen, J. M., Chen, H., Yang,  
898 X., Gao, W., and Geng, F. H.: Important role of ammonia on haze  
899 formation in Shanghai, *Environ. Lett.*, 6, 024019, 2011.

900 Yu, F. Q., Wang, Z., Luo, G., and Turco, R.: Ion-mediated nucleation as  
901 an important global source of tropospheric aerosols, *Atmos. Chem.*

902 Phys., 8, 2537-2554, 2008.

903 Yue. D. L., Hu. M., Zhang. R. J., Wu. Z. J., Su. H., et al.: Potential  
904 contribution of new particle formation to cloud condensation nuclei in  
905 Beijing, Atmos. Environ., 45, 6070-6077, 2011.

906 Yum. S. S., James, G. H., Keun, Y. S., and Byoung-Cheol, C.:  
907 Springtime cloud condensation nuclei concentrations on the west coast  
908 of Korea, Geophys. Res. Lett., 32, L09814, doi: 10.  
909 1029/2005GL022641, 2005.

910 Yum. S. S., and James, G. H.: Wintertime/summertime contrasts of cloud  
911 condensation nuclei and cloud microphysics over the South Ocean, J.  
912 Geophys. Res., 109, D06204, doi: 10.1029/2003JD003864, 2004.

913 Zhang, M., Wang, X., Chen, J., Cheng, T., Wang, T. et al.: Physical  
914 characterization of aerosol particles during the Chinese New Year's  
915 firework events, Atmos. Environ., 44, 5191-5198, 2010a.

916 Zhang, Q., Tie, X. X., Lin, W. L., Cao, J. J., Quan, J. N., Ran, L., and Xu,  
917 W. Y.: Variability of SO<sub>2</sub> in an intensive fog in North China Plain:  
918 Evidence of high solubility of SO<sub>2</sub>, Particuology, 11, 41-47, 2013.

919 Zhang, R. J., Jing, J. S., Tao, J., Hsu, S.-C., Wang, G., Cao, J. J., Lee, C. S.  
920 L., et al.: Chemical characterization and source apportionment of PM<sub>2.5</sub>  
921 in Beijing: seasonal perspective, Atmos. Chem. Phys., 13, 7053-7074,  
922 2013.

923 Zhang, X. Y., Zhuang G. S., Chen, J. M., Wang, Y. X., An, Z. S., Zhang, P.:

924 Heterogeneous reactions of sulfur dioxide on typical mineral particles, J.

925 Phys. Chem., B, 110, 12588-12596, 2006b.

926

927

928

929

930

931

932

933

934

935

936

937

938

939

940

941

942

943

944

945

946 **Table 1** Statistics of meteorological parameters in different weather  
 947 conditions.

	Clear day	Foggy-hazy day	Hazy day	All
Temperature ( °C)	14.4	14.6	16.6	15.0
Wind direction (deg)	157.2	191.4	260.6	191.3
Wind speed (m/s)	1.9	1.3	2.3	1.9
Pressure (hPa)	1021.9	1019.2	1019.5	1020.8
RH (%)	58.1	84.9	58.3	62.0
Visibility (km)	15.4	2.3	4.4	10.4
PBL (km)	1.2	0.65	0.62	1.01
Extinction coefficient (km <sup>-1</sup> )	0.42	0.71	0.78	0.55

948  
 949 **Table 2** Statistics of CCN, CN, CCN/CN and BC in different weather  
 950 conditions.

	Clear day	Foggy-hazy day	Hazy day	All
CCN range (cm <sup>-3</sup> )	994-5096	1677-2947	2088-6268	994-6268
CCN average (cm <sup>-3</sup> )	2432	2377	4362	2929
CN range (cm <sup>-3</sup> )	4270-15,168	4815-13,922	6033-15,771	4270-15,771
CN average (cm <sup>-3</sup> )	8956	8367	10500	9344
CCN/CN range	0.09-0.48	0.18-0.40	0.25-0.57	0.09-0.57
CCN/CN average	0.28	0.29	0.41	0.32
BC range (µg/m <sup>-3</sup> )	4.51-20.40	6.7-14.7	8.3-35.2	4.51-35.20
BC average (µg/m <sup>-3</sup> )	8.57	9.58	21.26	12.24

951  
 952  
 953 **Table 3** Effective hygroscopicity parameters ( $\kappa_i$ ), and densities of the  
 954 three category compositions in fine particles (Yue et al., 2011)

Species	Data source	$\kappa_i$	Density (g cm <sup>-3</sup> )
Sulfate & Nitrate	SO <sub>4</sub> <sup>2-</sup> +NO <sub>3</sub> <sup>-</sup> +NH <sub>4</sub> <sup>+</sup>	0.6	1.7
Sodium chloride and marine aerosols	Na <sup>+</sup> +Cl <sup>-</sup>	1.0	2.2
Insoluble compounds	BC	0	1.0
	others	0	2.0

955

956 **Figure captions**

957

958 **Figure 1** Agricultural fire scattering areas and air mass transport  
959 pathways across these regions. All red spots represent biomass burning  
960 sites on 7 November measured from MODIS satellite. Starting time (LT)  
961 is labeled in the figure.

962 **Figure 2** Temporal variations of temperature, wind speed and direction,  
963 RH, pressure and atmospheric visibility, the foggy-hazy case is marked in  
964 black open boxes and hazy case in red.

965 **Figure 3** Temporal variations of PBL and vertical extinction coefficient  
966 (500 m) measured by MPL lidar. Data from 5:00-9:00 on 7th are labeled  
967 as invalid and not shown. The foggy-hazy case is marked in red open  
968 boxes and hazy case in black.

969 **Figure 4** Hourly mean particle number concentrations of different  
970 sub-size bins, the foggy-hazy case is marked in red open boxes and hazy  
971 case in black.

972 **Figure 5** Average size distributions (10nm-1 $\mu$ m) for all the hazy,  
973 foggy-hazy, and clear cases.

974 **Figure 6** Temporal variations of particle water soluble ion composition  
975 and trace gases, the foggy-hazy case is marked in red open boxes and  
976 hazy case in black.

977 **Figure 7** Temporal variations of  $N_{CN}$ ,  $N_{CCN}$  at 0.2% SS, BC,  $PM_{2.5}$  and

978  $N_{CCN}/N_{CN}$ , the foggy-hazy case is marked in red open boxes and hazy  
979 case in black.

980 **Figure 8** Temporal variations of  $CN_{100nm-10\mu m}$ ,  $CN_{80nm-10\mu m}$ ,  $CCN/$   
981  $CN_{100nm-10\mu m}$  at 0.2% SS and  $CCN/ CN_{80nm-10\mu m}$  at 0.2% SS, the  
982 foggy-hazy case is marked in red open boxes and hazy case in black.

983 **Figure 9** Correlations of BC mass concentration ( $M_{BC}$ ) to  $N_{CCN}$  and  
984  $N_{CCN}/N_{CN}$  (0.2% SS).

985 **Figure 10** Scatterplot of the simplified closure analysis at SS 0.2%.

986 **Figure 11** Correlations of observed and predicted  $N_{CCN}$  (0.2% SS) in the  
987 clear (a) and foggy-hazy/hazy (b) cases.

988

989

990

991

992

993

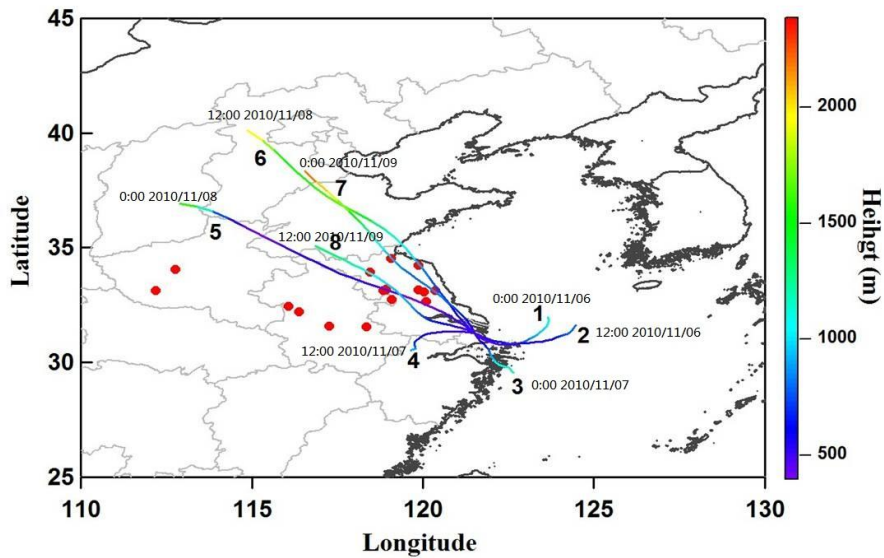
994

995

996

997

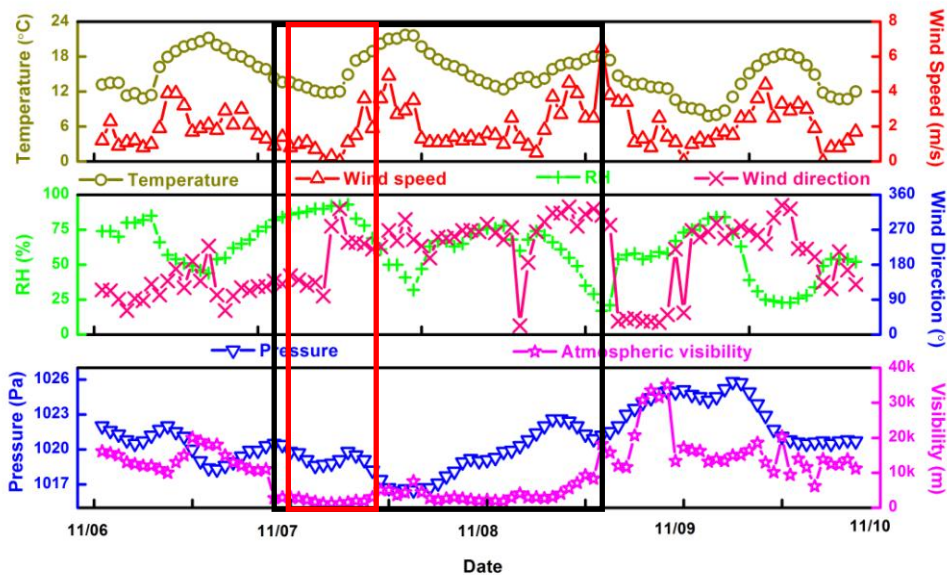
998



999

1000 **Figure 1** Agricultural fire scattering areas and air mass transport  
 1001 pathways across these regions. All red spots represent biomass burning  
 1002 sites on 7 November measured from MODIS satellite. Starting time (LT)  
 1003 is labeled in the figure.

1004



1011

1012 **Figure 2** Temporal variations of temperature, wind speed and direction,  
 1013 RH, pressure and atmospheric visibility, the foggy-hazy case is marked in  
 1014 red open boxes and hazy case in black.

1015

1016

1017

1018

1019

1020

1021

1022

1023

1024

1025

1026

1027

1028

1029

1030

1031

1032

1033

1034

1035

1036

1037

1038

1039

1040

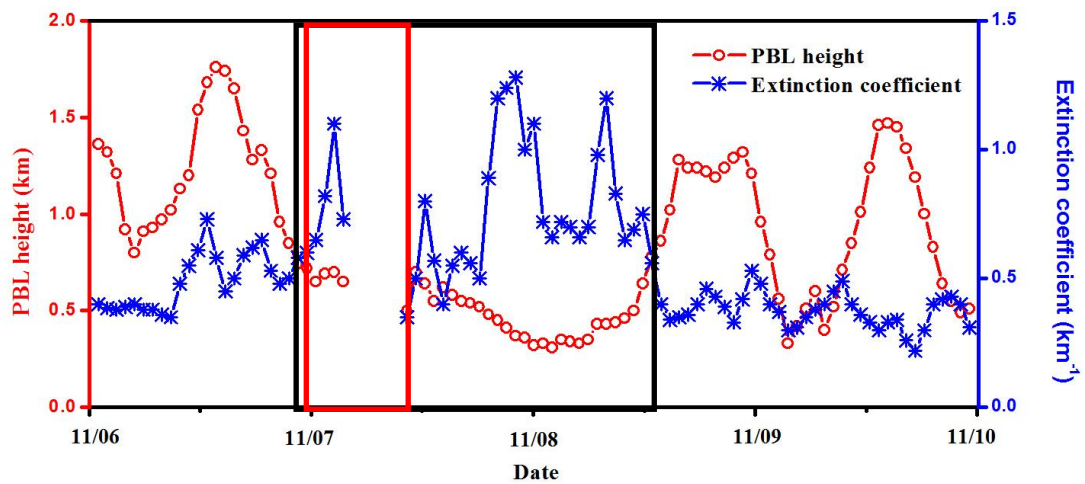


**Figure 3** Temporal variations of PBL and vertical extinction coefficient (500 m) measured by MPL lidar. Data from 5:00-9:00 on 7th are labeled as invalid and not shown. The foggy-hazy case is marked in red open boxes and hazy case in black.

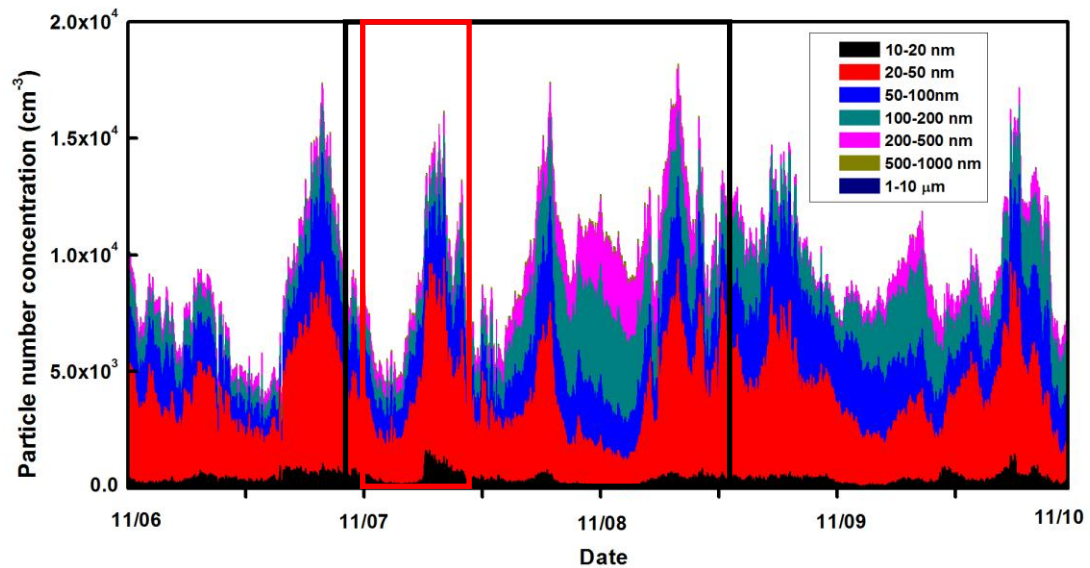


**Figure 4** Hourly mean particle number concentrations of different sub-size bins, the foggy-hazy case is marked in red open boxes and hazy case in black.



1041

1042

1043

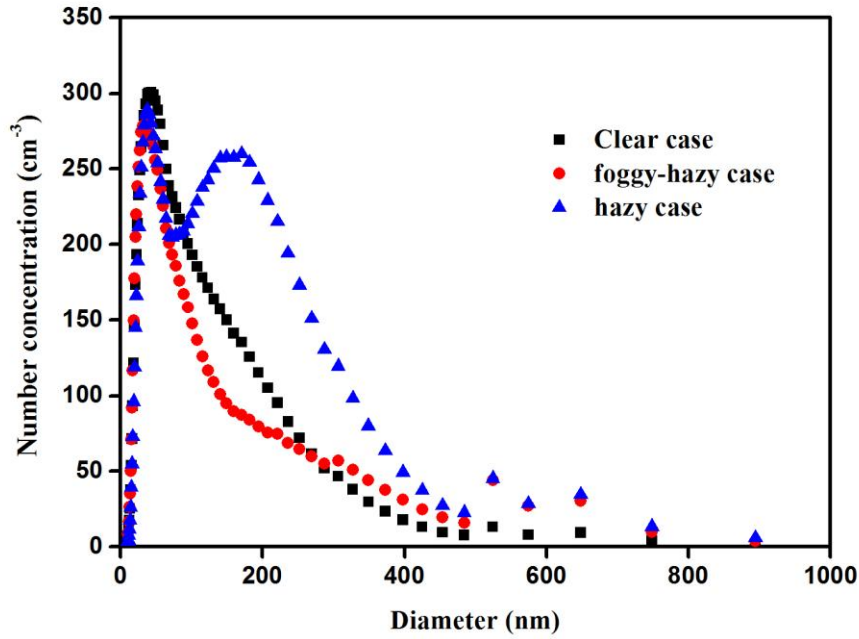
1044

1045

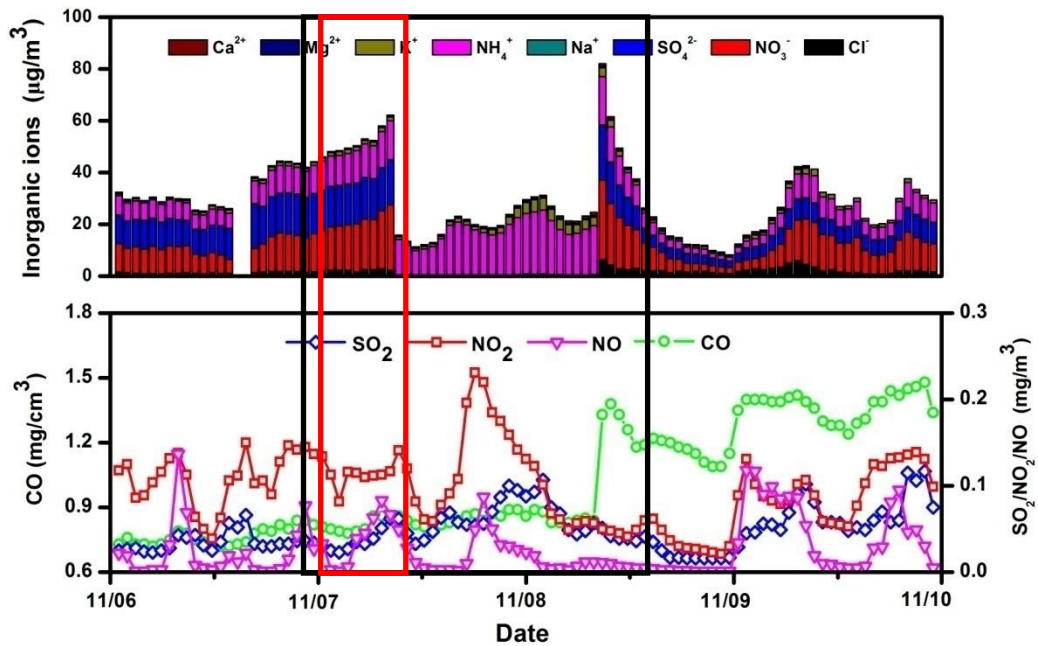
1046

1047

1048



1049 **Figure 5** Average size distributions (10nm-1µm) for all the hazy,  
1050 foggy-hazy, and clear cases.



1051

1052 **Figure 6** Temporal variations of particle water soluble ion composition  
1053 and trace gases, the foggy-hazy case is marked in red open boxes and  
1054 hazy case in black.

1055

1056

1057

1058

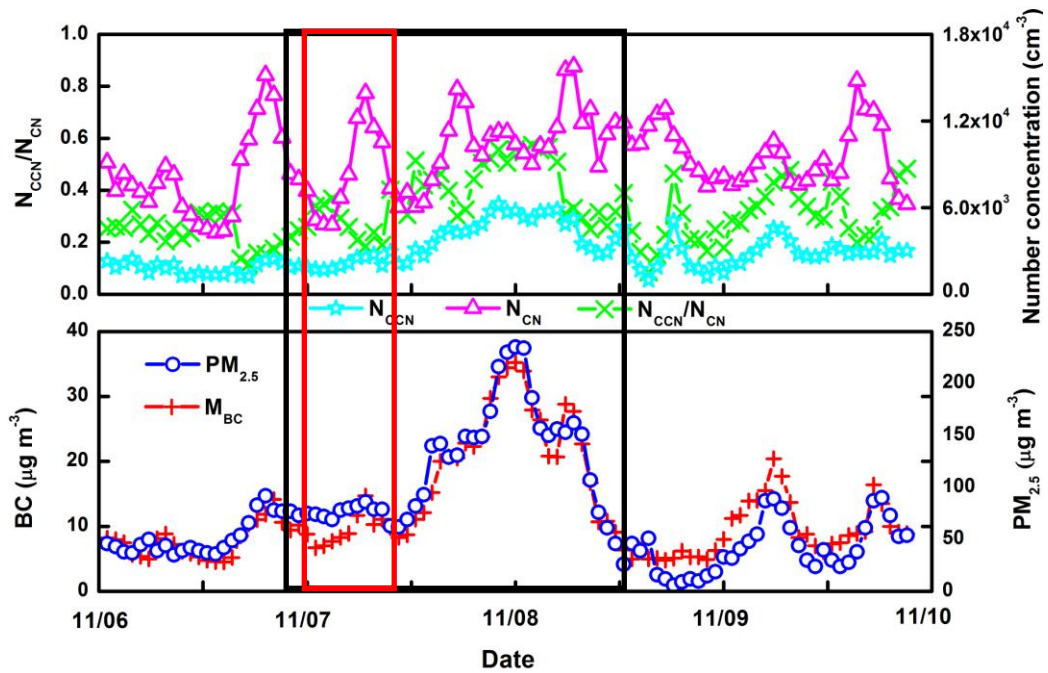
1059

1060

1061

1062

1063



1064 **Figure 7** Temporal variations of  $N_{CN}$ ,  $N_{CCN}$  at 0.2% SS, BC,  $PM_{2.5}$  and

1065  $N_{CCN}/N_{CN}$ , the foggy-hazy case is marked in red open boxes and hazy

1066 case in black.

1067

1068

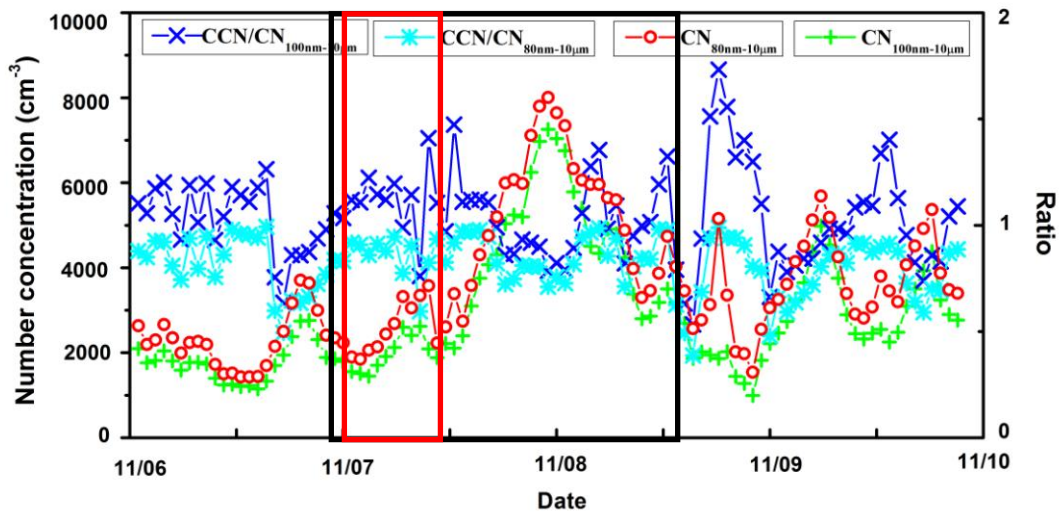
1069

1070

1071

1072

1073

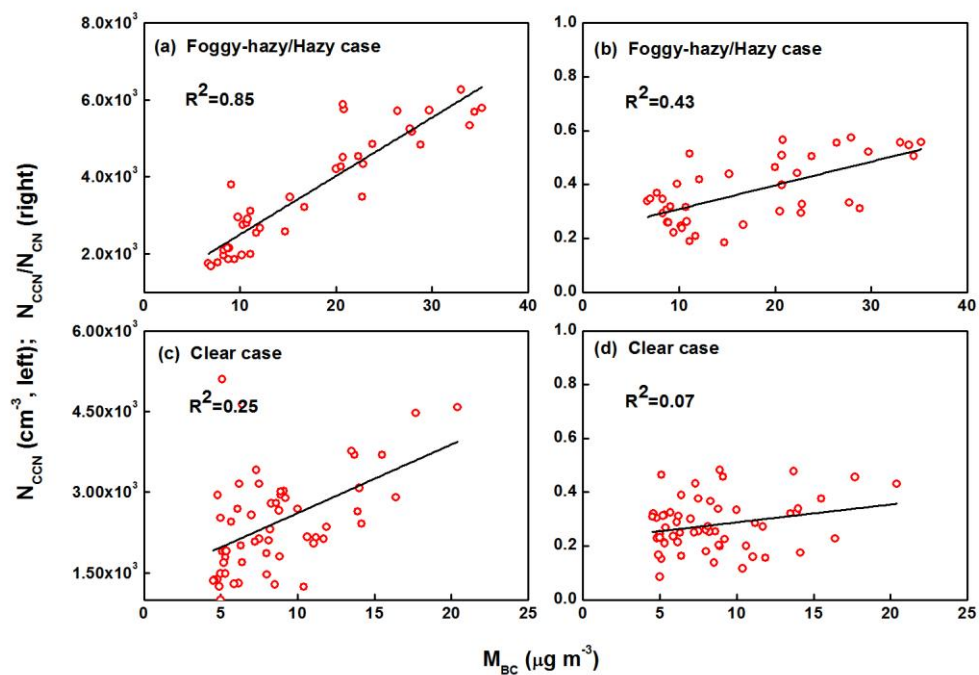


1074 **Figure 8** Temporal variations of  $CN_{100nm-10\mu m}$ ,  $CN_{80nm-10\mu m}$ ,  $CCN/$

1075  $CN_{100nm-10\mu m}$  at 0.2% SS and  $CCN/ CN_{80nm-10\mu m}$  at 0.2% SS, the

1076 foggy-hazy case is marked in red open boxes and hazy case in black.

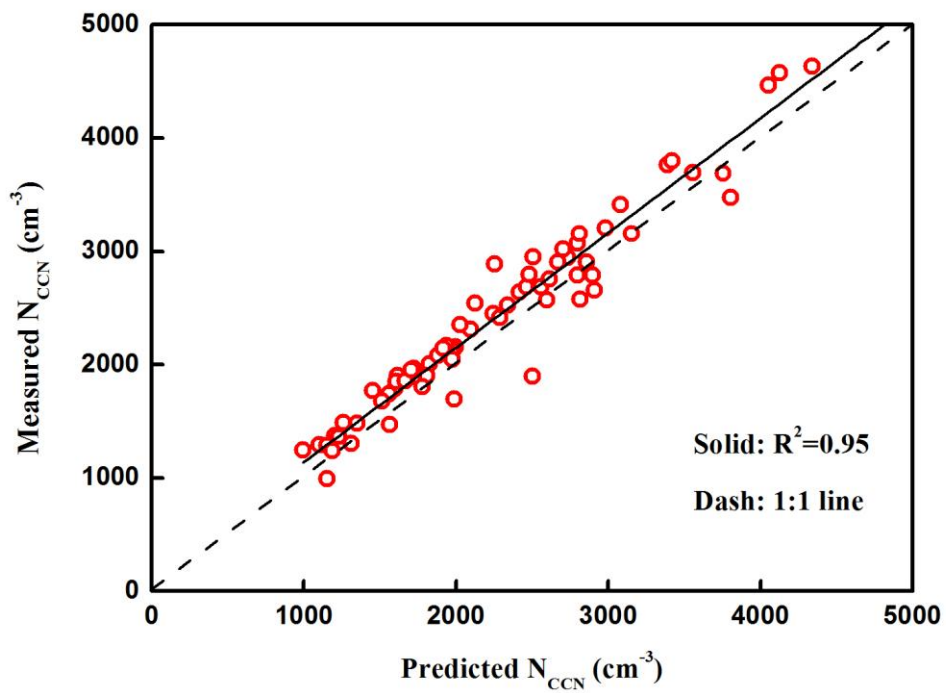
1077



1078

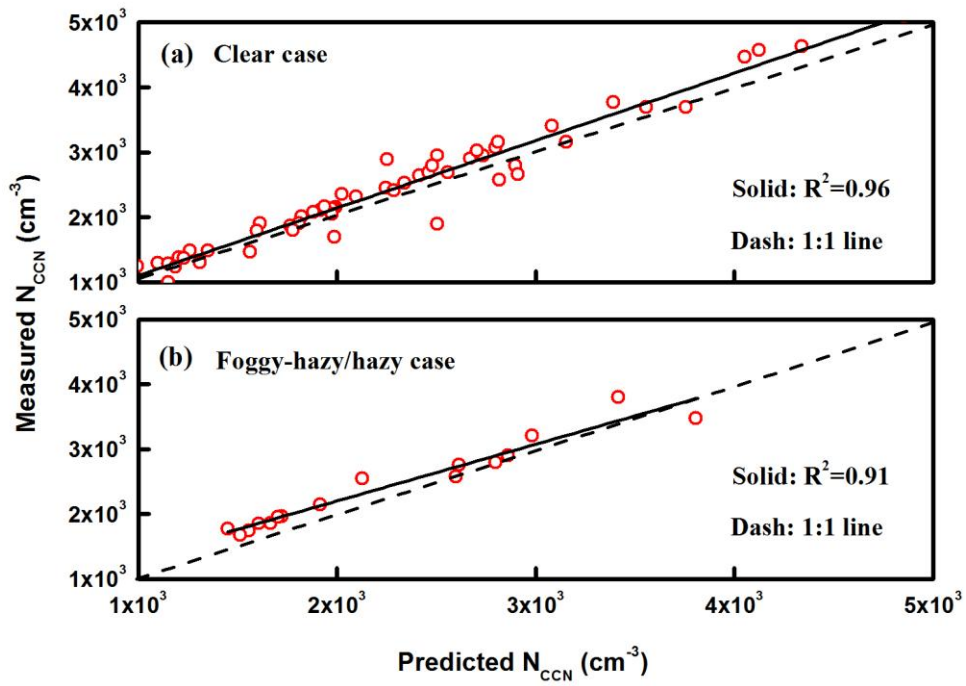
1079 **Figure 9** Correlations of BC mass concentration ( $M_{BC}$ ) to  $N_{CCN}$  and

1080  $N_{CCN}/N_{CN}$  (0.2% SS).



1081

1082 **Figure 10** Scatterplot of the simplified closure analysis at SS 0.2%.



1083

1084 **Figure 11** Correlations of observed and predicted  $N_{CCN}$  (0.2% SS) in the  
 1085 clear (a) and foggy-hazy/hazy (b) cases.

1086

1087